# 1 Correlated Electrons: Why we need Models to Understand Real Materials?

Alexander Lichtenstein
I. Institut für Theoretische Physik
Universität Hamburg, 20355 Hamburg, Germany

## Contents



E. Pavarini, E. Koch, F. Anders, and M. Jarrell
Correlated Electrons: From Models to Materials
Modeling and Simulation Vol. 2
Forschungszentrum Jülich, 2012, ISBN 978-3-89336-796-2
http://www.cond-mat.de/events/correl12

# 1 Introduction

The technical inventions of the last century are closely related with the design of silicon based materials for the semiconductor industry. The theoretical development of the last fifty years and the associated success in describing electronic properties of such weakly correlated materials started with the conception of the density functional theory (DFT), which was initiated by seminal works of Walter Kohn, Pierre Hohenberg, and Lu Sham [1, 2]. This is the first-principles scheme based on the exact theorem, stating that the ground state of interacting electron systems can be found by minimizing an universal functional of the density in some additional external field. The main problem of DFT is related with the fact, that this functional is not known in general and can be calculated numerically with a reasonable accuracy only for the simple case of the homogeneous electron gas. These calculations, which have been proven to be very useful for the DFT scheme, have been done by David Ceperley and Berni Alder [3] using the two-step quantum Monte Carlo procedure starting from the "fixed-node" approximation followed by a "released-node" calculation. Nevertheless the accuracy of such scheme is still limited and is very sensitive to the computational details [4]. The main restriction of the density functional scheme is the fact that it only gives ground state properties, while spectral information can be found only in the time-dependent DFT scheme [5]. While the structural relaxation of complex materials can be carried out very efficiently in the generalized gradient approximation of the DFT, due to almost spherical properties of the exchange-correlation hole [6], the quality of spectral properties crucially depends on systems in question. The TDFT scheme has more problems than the static DFT approach, since there are no suitable time-dependent reference systems to find an exchange correlation kernel.

The enormous progress of the last three decades in designing completely new materials for high-$T_c$ superconductivity, giant and colossal magnetoresistance, or artificially created two-dimensional lattices brings new importance to the theory of transition-metal systems. It turns out that even the ground state properties of antiferromagnetic oxides or orbitally ordered com-

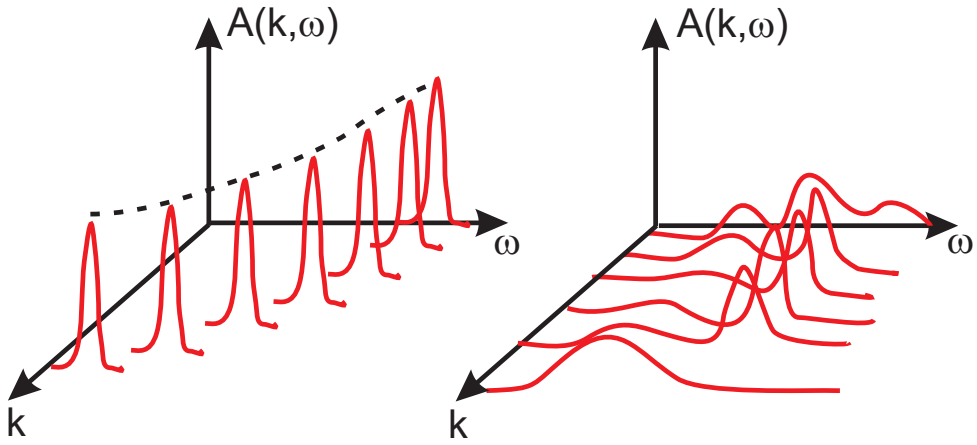


**Fig. 1:** *Schematic view of angular-resolved photoemission spectra (ARPES) for normal (left) and correlated electron materials (right).*

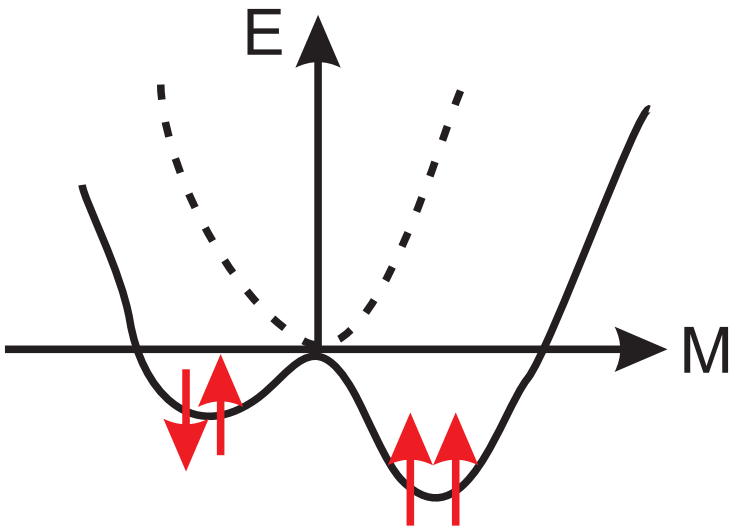


**Fig. 2:** *Schematic representation of spin (as well as charge or orbital) fluctuations in correlated electron systems.*

pounds are not described well in the DFT scheme [7]. The accurate angle-resolved photoemission study of the cuprate superconductors clearly shows, that the spectral properties of such systems, with strong electron-electron interactions in the $3d$-shell of transition metals has well pronounced incoherent features [8]. We present in Fig. 1 the qualitative difference between the spectral function of normal metals with well-defined quasiparticle peaks at all momenta $\mathbf{k}$ and the strongly correlated case with an incoherent part and a non-quasiparticle spectrum in the Brillouin zone.

The main source of complex correlated behavior of electronic systems, related with strong fluctuations between different low-energy fermionic configurations, is shown schematically in Fig. 2. For example, if the free energy of an electronic system has only one well defined minimum at zero local moment (the dashed curve) then one can expect small electron fluctuations and normal paramagnetic quasiparticle behavior. In the case of two low-lying minima corresponding to singlet and triplet excitations (solid curve) one can expect strong many-body fluctuations and possibly non-quasiparticle behavior related with local so-called Hund's rule physics [9]. In order to treat the system with such effective energy profiles, we need to use the path-integral approach and calculate the corresponding correlation functions using complicated quantum Monte Carlo schemes, which can handle many local minima in the free-energy functional on an equal footing.

In this lecture we review the general functional approach to strongly correlated electron systems, discuss an elegant way to separate the local and non-local correlations, and show how one can solve the local correlation problem using the recently developed continuous time Monte Carlo (CT-QMC) scheme. Finally we show an efficient way to go from the simple model investigations of strongly correlated systems to realistic investigation of complex electronic materials.

# 2 Functional approach: Route to fluctuations

We introduce a general functional approach which will cover Density Functional (DFT), Dynamical Mean-Field (DMFT), and Baym-Kadanoff (BK) Theory [10]. Let us start from the full many–body Hamiltonian describing electrons moving in the periodic external potential of ions $V(\mathbf{r})$, with chemical potential $\mu$, and interacting via Coulomb law: $U(\mathbf{r}-\mathbf{r}') = 1/|\mathbf{r}-\mathbf{r}'|$. We use atomic units $\hbar = m = e = 1$. In the field-operator representation the Hamiltonian takes the form

$$\begin{aligned} H &= \sum_{\sigma} \int d\mathbf{r}\, \hat{\psi}^{\dagger}_{\sigma}(\mathbf{r}) \left( -\frac{1}{2}\nabla^2 + V(\mathbf{r}) - \mu \right) \hat{\psi}_{\sigma}(\mathbf{r}) \\ &+ \frac{1}{2} \sum_{\sigma\sigma'} \int d\mathbf{r} \int d\mathbf{r}'\, \hat{\psi}^{\dagger}_{\sigma}(\mathbf{r}) \hat{\psi}^{\dagger}_{\sigma'}(\mathbf{r}')\, U(\mathbf{r}-\mathbf{r}')\, \hat{\psi}_{\sigma'}(\mathbf{r}') \hat{\psi}_{\sigma}(\mathbf{r}). \end{aligned} \tag{1}$$

We can always use a single-particle orthonormal basis set $\phi_n(\mathbf{r})$, for example Wannier orbitals, with a full set of quantum numbers, e.g., site, orbital and spin index: $n = (im\sigma)$ and expand the fields in creation and annihilation operators

$$\begin{aligned} \hat{\psi}(\mathbf{r}) &= \sum_{n} \phi_n(\mathbf{r}) \hat{c}_n \\ \hat{\psi}^{\dagger}(\mathbf{r}) &= \sum_{n} \phi^*_n(\mathbf{r}) \hat{c}^{\dagger}_n \end{aligned} \tag{2}$$

Going from fermionic operators to the Grassmann variables $\{c^*_n,\, c_n\}$, we can write the functional integral representation of the partition function of the many-body Hamiltonian in the imaginary time domain using the Euclidean action $S$

$$Z = \int \mathcal{D}[c^*, c] e^{-S} \tag{3}$$

$$S = \sum_{12} c^*_1 \, (\partial_\tau + t_{12}) \, c_2 + \frac{1}{4} \sum_{1234} c^*_1 c^*_2 \, U_{1234} \, c_4 c_3 \,, \tag{4}$$

where the one- and two-electron matrix elements are defined as

$$\begin{aligned} t_{12} &= \int d\mathbf{r}\, \phi^*_1(\mathbf{r}) \left( -\frac{1}{2}\bigtriangledown^2 + V(\mathbf{r}) - \mu \right) \phi_2(\mathbf{r}) \\ U_{1234} &= \int d\mathbf{r} \int d\mathbf{r}'\, \phi^*_1(\mathbf{r}) \phi^*_2(\mathbf{r}')\, U(\mathbf{r}-\mathbf{r}')\, \phi_3(\mathbf{r}) \phi_4(\mathbf{r}'). \end{aligned} \tag{5}$$

and we use the following short definition of the sum:

$$\sum_{1} ... \equiv \sum_{im} \int d\tau ... \tag{6}$$

The one-electron Green function is defined via a simplest non-zero correlation function

$$G_{12} = -\langle c_1 c^*_2 \rangle_S = -\frac{1}{Z} \int \mathcal{D}[c^*, c]\, c_1 c^*_2\, e^{-S} \tag{7}$$

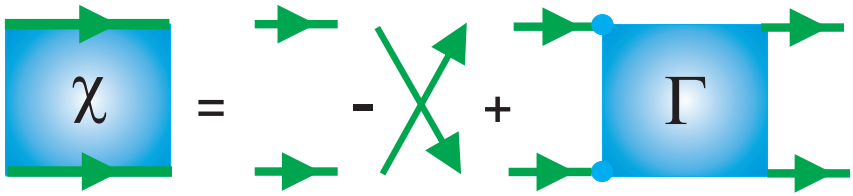


**Fig. 3:** *Representation of the full two-particle Green function in terms single-particle Green functions and the full vertex function $\Gamma$.*

The main problems of strongly interacting electronic systems are related to the fact that the higher order correlation functions do not separate into a product of lower order correlation functions. For example the two-particle Green function or generalized susceptibilities, $\chi$, are defined in the following form [11]

$$\chi_{1234} = \langle c_1 c_2 c_3^* c_4^* \rangle_S = \frac{1}{Z} \int \mathcal{D}[c^*, c]\, c_1 c_2 c_3^* c_4^*\, e^{-S}\,, \tag{8}$$

and can be expressed graphically through Green functions and the full vertex function $\Gamma_{1234}$ [12] as shown in Fig. 3

$$X_{1234} = G_{14}G_{23} - G_{13}G_{24} + \sum_{1'2'3'4'} G_{11'}G_{22'}\Gamma_{1'2'3'4'}G_{3'3}G_{4'4} \tag{9}$$

In the case of non-interacting electron systems, the high-order correlations $\chi$ are reduced to the antisymmetrized products of lower-order correlations $G$, which would correspond to the first two terms (Hartree and Fock like) with the vertex function $\Gamma$ in Eq. (9) equal to zero. In strongly correlated electron systems the last part with the vertex is dominant and even diverges close to an electronic phase transition.

The Baym-Kadanoff functional [13] gives the one-particle Green function and the total free energy at its stationary point. In order to construct the exact functional of the Green function (Baym-Kadanoff), we modify the action by introducing the source term $J$

$$S[J] = S + \sum_{ij} c_i^* J_{ij} c_j\,. \tag{10}$$

The partition function $Z$, or equivalently the free energy of the system $F$, becomes a functional of the auxiliary source field

$$Z[J] = e^{-F[J]} = \int \mathcal{D}[c^*, c]\, e^{-S[J]}\,. \tag{11}$$

Variation of this source function gives all correlation functions, for example the Green function

$$G_{12} = \frac{1}{Z[J]} \frac{\delta Z[J]}{\delta J_{12}}\bigg|_{J=0} = \frac{\delta F[J]}{\delta J_{12}}\bigg|_{J=0}\,. \tag{12}$$

Likewise, the generalized susceptibility $\chi$ is obtained as a second variation of the partition function $Z[J]$. The second variation of the free energy functiontional $F[J]$ gives the connected part of the $\chi$-function, which is the last term of Eq. (9).

The Baym–Kadanoff functional can be obtained by Legendre transforming from $J$ to $G$

$$F[G] = F[J] - \mathrm{Tr}(JG), \tag{13}$$

We can use the standard decomposition of the free energy $F$ into the single particle part and the correlated part

$$F[G] = \mathrm{Tr}\ln G - \mathrm{Tr}\,(\Sigma G) + \Phi[G], \tag{14}$$

were $\Sigma_{12}$ is single particle self-energy and $\Phi[G]$ is a correlated part of the Baym–Kadanoff functional and is equal to the sum of all two-particle irreducible diagrams. At its stationary point this functional gives the free energy of the system. One can use a different Legendre transform and obtain functionals of the self-energy $\Sigma$ [14], or complicated functionals of two variables $G$ and $\Gamma$ [15], or a more simple functional of $G$ and screened Coulomb interactions $W$ [10] which is useful in GW theory.

In practice, $\Phi[G]$ is not known for interacting electron systems, which is similar to the problem of the unknown universal functional in density functional theory. Moreover, this general functional approach reduces to the DFT theory, if one only uses the diagonal part in the space-time representation of the Green function, which corresponds to the one-electron density

$$n_1 = G_{12}\delta_{12} = \langle c_1^* c_1 \rangle_S, \tag{15}$$

with the Kohn-Sham potential $V_{KS} = V_{ext} + V_H + V_{xc}$ playing the role of the"constrained field" $J$. In this case we lose information about the non equal-time Green's function, which gives the single-particle excitation spectrum as well as the k-dependence of the spectral function, and we restrict ourselves to only the ground state energy of the many-electron system. Moreover, we also lose information about all collective excitations in solids, such as plasmons or magnons, which can be obtained from a generalized susceptibility or from the second variation of the free energy.

One can probably find the Baym-Kadanoff interacting potential $\Phi[G]$ for simple lattice models using quantum Monte Carlo (QMC). Unfortunately, due to the sign problem in lattice simulations, this numerically exact solution of electronic correlation problem is not possible. On the other hand, one can obtain the solution of local interacting quantum problem in a general fermionic bath, using a QMC scheme, which has no sign problem if it is diagonal in spin and orbital space. Therefore, a reasonable approach to strongly correlated systems is to keep only a local part of the many-body fluctuations. In such a Dynamical Mean-Field Theory (DMFT) one can obtain numerically the correlated part of the local functional. In this scheme we only use the local part of the many-electron vertex and obtain, in a self-consistent way, an effective functional of the local Green function. In the following section we discuss the general dual-fermion (DF) transformations [16] which will help us to separate the local fluctuations in many-body system and show a perturbative way to go beyond the DMFT approximations.

# 3 Local correlations and beyond

We will only consider the local, but multiobital, interaction vertex $U^i_{mm'm''m'''}$. Sometimes we will omit all orbital indices for simplicity. All equations will be written in matrix form, giving the idea of how to generalize a dual-fermion (DF) scheme to the multi-orbital case [17,18]. The general strategy to separate the local and non-local correlations effects is associated with the introduction of auxiliary fermionic fields which will couple separated local correlated impurities models back to the lattice [16]. In order to include the smaller non-local part of the Coulomb interactions one can use a more general approach using auxiliary fermionic and bosonic fields [19].

We rewrite corresponding original action, Eq. (3), in Matsubara space as a sum of the non-local one-electron contribution with $t_{12}$ and the local interaction part $U$

$$S[c^*,c] = -\sum_{\omega\mathbf{k}\sigma\, mm'} c^*_{\omega\mathbf{k}\sigma m}\left[(i\omega+\mu)\mathbf{1} - t^{mm'}_{\mathbf{k}\sigma}\right] c_{\omega\mathbf{k}\sigma m'} + \sum_i S_{\mathrm{U}}[c^*_i, c_i]. \tag{16}$$

The index $i$ labels the lattice sites, $m$ refers to different orbitals, $\sigma$ is the spin projection and the $\mathbf{k}$-vectors are quasi-momenta. In order to keep the notation simple, it is useful to introduce the combined index $\alpha \equiv \{m,\sigma\}$. Translational invariance is assumed for simplicity in the following, although a real space formulation is straightforward. The local part of the action, $S_{\mathrm{U}}$, may contain any type of local multi-orbital interaction.

In order to formulate an expansion around the best possible auxiliary local action, a quantum impurity problem is introduced

$$S_{\mathrm{loc}}[c^*,c] = -\sum_{\omega\,\alpha\beta} c^*_{\omega\alpha}\left[(i\omega+\mu)\mathbf{1} - \Delta^{\alpha\beta}_{\omega}\right] c_{\omega\beta} + S_{\mathrm{U}}[c^*,c], \tag{17}$$

where $\Delta_\omega$ is the effective hybridization matrix describing the coupling of the impurity to an auxiliary fermionic bath. The main motivation for rewriting the lattice action in terms of a quantum impurity model is that such a reference system can be solved numerically exactly for an arbitrary hybridization function using the CT-QMC methods [20]. Using the locality of the hybridization function $\Delta_\omega$, the lattice action (16) can be rewritten exactly in terms of individual impurity models and the effective one-electron coupling $(t_{ij} - \Delta_\omega)$ between different impurities

$$S[c^*,c] = \sum_i S_{\mathrm{loc}}[c^*_i, c_i] + \sum_{\omega\mathbf{k}\,\alpha\beta} c^*_{\omega\mathbf{k}\alpha}\left(t^{\alpha\beta}_{\mathbf{k}} - \Delta^{\alpha\beta}_{\omega}\right) c_{\omega\mathbf{k}\beta}. \tag{18}$$

We will find the condition for the optimal choice of the hybridization function later. Although we can solve the individual impurity model exactly, the effect of spatial correlations due to the second term in Eq. (18) is very hard to treat, even perturbatively, since the impurity action is non-Gaussian and one cannot use the Wick theorem. The main idea of a dual-fermion transformation is the change of variables from $(c^*, c)$ to weakly correlated Grassmann fields $(f^*, f)$ in the path integral representation of the partition function, Eq. (3), followed by a simple perturbative treatment. The new variables are introduced through the Hubbard-Stratonovich

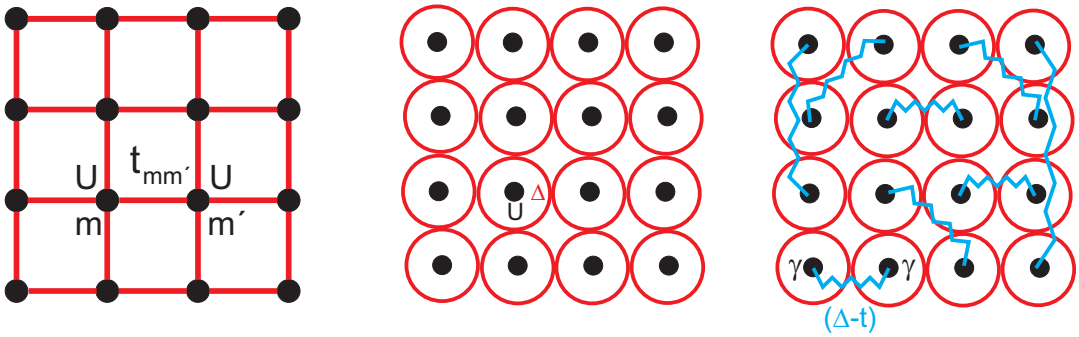


**Fig. 4:** *From the lattice model (left) via real-space DMFT (middle) to the non-local dual-fermion perturbation (right).*

transformation

$$\exp\left(c^*_\alpha b_\alpha (M^{-1})_{\alpha\beta} b_\beta c_\beta\right) = \frac{1}{\det M} \int \mathcal{D}[f^*, f] \exp\left(-f^*_\alpha M_{\alpha\beta} f_\beta - c^*_\alpha b_\alpha f_\alpha - f^*_\beta b_\beta c_\beta\right). \quad (19)$$

In order to transform the exponential of the bilinear term in (18), we choose the matrices $M_{\alpha\beta}$, and scaling function $b_\alpha$ (if we assume for simplicity that the local Green's function is diagonal in orbital and spin space) in accordance with Refs. [16] as

$$M = g_\omega^{-1} \left(\Delta_\omega - t_{\mathbf{k}}\right)^{-1} g_\omega^{-1}, \qquad b = g_\omega^{-1}, \quad (20)$$

where $g_\omega$ is the local, interacting Green function of the impurity problem

$$g_{12} = -\langle c_1 c^*_2 \rangle_{\text{loc}} = -\frac{1}{\mathcal{Z}_{\text{loc}}} \int \mathcal{D}[c^*, c] c_1 c^*_2 \exp\Big(-S_{\text{loc}}[c^*, c]\Big). \quad (21)$$

With this choice, the lattice action transforms to

$$S[c^*, c, f^*, f] = \sum_i S^i_{\text{site}} + \sum_{\omega \mathbf{k}\, \alpha\beta} f^*_{\omega \mathbf{k}\alpha} [g_\omega^{-1} \left(\Delta_\omega - t_{\mathbf{k}}\right)^{-1} g_\omega^{-1}]_{\alpha\beta} f_{\omega \mathbf{k}\beta}. \quad (22)$$

Hence the coupling between sites is transferred to a local coupling to the auxiliary fermions

$$S^i_{\text{site}}[c^*_i, c_i, f^*_i, f_i] = S_{\text{loc}}[c^*_i, c_i] + \sum_{\alpha\beta} f^*_{\omega i\alpha}\, g^{-1}_{\omega\,\alpha\beta} c_{\omega i\beta} + c^*_{\omega i\alpha}\, g^{-1}_{\omega\,\alpha\beta} f_{\omega i\beta}. \quad (23)$$

Since $g_\omega$ is local, the sum over all states labeled by $\mathbf{k}$ can be replaced by a summation over all sites by a change of basis in the second term. The crucial point is that the coupling to the auxiliary fermions is purely local and $S_{\text{site}}$ decomposes into a sum of local terms. The lattice fermions can therefore be integrated-out from $S_{\text{site}}$ for each site $i$ separately. This completes the change of variables

$$\int \mathcal{D}[c^*, c] \exp\left(-S_{\text{site}}[c^*_i, c_i, f^*_i, f_i]\right) = \mathcal{Z}_{\text{loc}} \exp\Big(-\sum_{\omega\,\alpha\beta} f^*_{\omega i\alpha}\, g^{-1}_{\omega\,\alpha\beta} f_{\omega i\beta} - V_i[f^*_i, f_i]\Big). \quad (24)$$

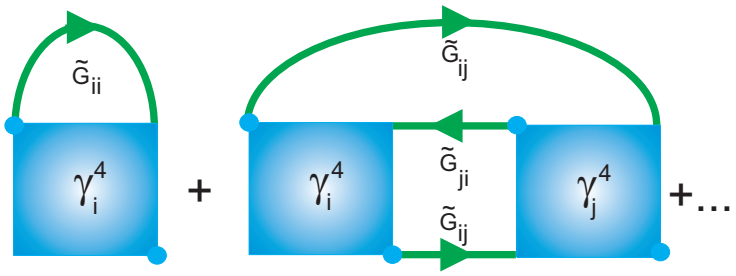


**Fig. 5:** *Diagrams contributing to the dual self-energy $\tilde{\Sigma}$.*

The above equation may be viewed as the defining equation for the dual potential $V[f^*, f]$. The choice of matrices (20) ensures a particularly simple form of this potential. An explicit expression is found by expanding both sides of Eq. (24) and equating the resulting expressions order by order. Formally this can be done to all orders and in this sense the transformation to the dual-fermions is exact. For most applications, the dual potential is approximated by the first non-trivial interaction vertex

$$V[f^*, f] = \frac{1}{4}\,\gamma_{1234}\, f_1^* f_2^* f_4 f_3, \tag{25}$$

where the combined index $1 \equiv \{\omega\alpha\}$ comprises frequency, spin and orbital degrees of freedom. $\gamma$ is the exact, fully antisymmetric, reducible two-particle vertex of the local quantum impurity problem. It is given by

$$\gamma_{1234} = g^{-1}_{11'} g^{-1}_{22'} \left[\chi_{1'2'3'4'} - \chi^0_{1'2'3'4'}\right] g^{-1}_{3'3} g^{-1}_{4'4}, \tag{26}$$

with the two-particle Green function of the impurity being defined as

$$\chi_{1234} = \langle c_1 c_2 c_3^* c_4^* \rangle_{\text{loc}} = \frac{1}{Z_{\text{loc}}} \int \mathcal{D}[c^*, c]\; c_1 c_2 c_3^* c_4^*\; e^{-S_{\text{loc}}[c^*, c]}\;. \tag{27}$$

The disconnected part reads

$$\chi^0_{1234} = g_{14} g_{23} - g_{13} g_{24}\;. \tag{28}$$

The single- and two-particle Green functions can be calculated using the CT-QMC [20]. After integrating-out the lattice fermions, the dual action depends only on the new variables

$$\tilde{S}[f^*, f] = -\sum_{\omega \mathbf{k}\, \alpha\beta} f^*_{\omega\mathbf{k}\alpha} [\tilde{G}^0_\omega(\mathbf{k})]^{-1}_{\alpha\beta} f_{\omega\mathbf{k}\beta} + \sum_i V_i[f_i^*, f_i]. \tag{29}$$

and the bare dual Green function involves the local Green function $g_\omega$ of the impurity model

$$\tilde{G}^0_\omega(\mathbf{k}) = \left[g_\omega^{-1} + \Delta_\omega - t_{\mathbf{k}}\right]^{-1} - g_\omega\;. \tag{30}$$

Up to now, Eqs. (29) and (30) are mere reformulations of the original problem. In practice, approximate solutions are constructed by treating the dual problem perturbatively. Several diagrams contributing to the dual self-energy are shown in Fig. 5. These are constructed from the impurity vertices and dual Green functions. The first diagram is purely local, while higher

orders contain nonlocal contributions, e.g., the second diagram in Fig. 5. In practice, approximations to the self-energy are constructed in terms of skeleton diagrams. The lines shown in Fig. 5 are therefore understood to be fully dressed propagators. The use of skeleton diagrams is necessary to ensure that the resulting theory is conserving in the Baym-Kadanoff sense [13], i.e., it fulfills the basic conservation laws for energy, momentum, spin, and particle number. The most useful property of such dual perturbation theory is good convergence both in the weak-coupling limit, when the local vertex is small and in the strong-coupling limit, when the dual Green's function is small [21].

The hybridization function $\Delta$, which so far has not been specified, allows to optimize the starting point of the perturbation theory and should be chosen in an optimal way. The condition of the first diagram (Fig. 5) as well as all local diagrams with higher-order correlation functions in the expansion of the dual self-energy to be equal to zero at all frequencies, fixes the hybridization. This eliminates the leading-order diagrammatic correction to the self-energy and establishes a connection to DMFT, which can be seen as follows: Since the $\gamma$ vertex is local, this condition amounts to demanding that the local part of the dual Green function be zero

$$\sum_{\mathbf{k}} \tilde{G}_{\omega}(\mathbf{k}) = 0. \tag{31}$$

The simplest nontrivial approximation is obtained by taking the leading-order correction, the first diagram in Fig. 5, evaluated with the bare dual propagator (30). Using the expression for the DMFT Green function [22]

$$G^{\mathrm{DMFT}}_{\omega}(\mathbf{k}) = \left[g^{-1}_{\omega} + \Delta_{\omega} - t_{\mathbf{k}}\right]^{-1}, \tag{32}$$

it immediately follows that (31) evaluated with the bare dual Green function is exactly equivalent to the DMFT self-consistency condition for $\Delta_{\omega}$

$$\frac{1}{N_k}\sum_{\mathbf{k}} G^{\mathrm{DMFT}}_{\omega}(\mathbf{k}) = g_{\omega}\,. \tag{33}$$

In the limit of infinitely large lattice connectivity the DMFT scheme becomes exact with the local self-energy [23]. The DMFT approximation for real lattice models appears to be one of the most successful many body schemes for realistic multi orbital systems [10]. Since it involves the exact solution of the many-body multi-orbital impurity model Eq. (21) all local quantum fluctuations of different orbitals, spins, and charges (Fig. 6) are included in this scheme.

In the DMFT approach one can study paramagnetic correlated phases of complex crystals with strong spin and orbital fluctuations above transition temperatures of the spin- and orbital-ordered states [24].

Hence DMFT appears as the zero-order approximation in this approach and corrections to DMFT are included perturbatively. A formal relation to DMFT can be established using the Feynman variational functional approach. In this context, DMFT appears as the optimal approximation to a Gaussian ensemble of dual fermions [25].

When diagrammatic corrections are taken into account and the first diagram is evaluated with the dressed propagator $\tilde{G}$, the condition (31) will in general be violated. It can be reinforced

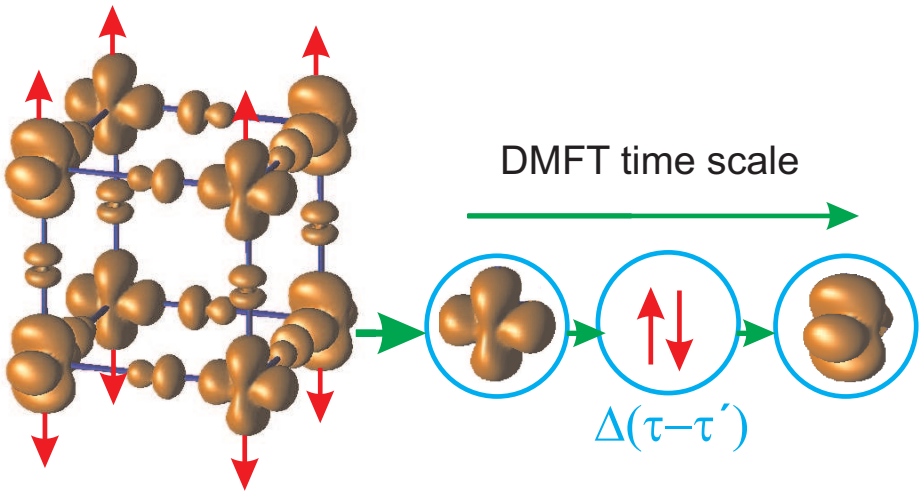


**Fig. 6:** *Schematic representations of initial lattice model (left) and the local DMFT approach with orbital and spin fluctuations (right).*

by adjusting the hybridization function iteratively. This corresponds to eliminating an infinite partial series of all local diagrams, starting from the first term in Fig. 5. These contributions are effectively absorbed into the impurity problem. Note that such an expansion is not one around DMFT, but rather around an optimized impurity problem.

The only difference between a DMFT and a DF calculation are the diagrammatic corrections which are included into the dual Green function. To this end, the local impurity vertex $\gamma$ has to be calculated in addition to the Green function in the impurity solver step.

It is an important consequence of the exact transformation (19) that for a theory, which is conserving in terms of dual fermions, the result is also conserving in terms of lattice fermions [25]. This allows to construct general conserving approximations within the dual fermion approach. Numerically, the self-energy is obtained in terms of skeleton diagrams by performing a self-consistent renormalization as described below. Once an approximate dual self-energy is found, the result may be transformed back to a physical result in terms of lattice fermions using exact relations.

The action (29) allows for a Feynman-type diagrammatic expansion in powers of the dual potential $V$. The rules are similar to those of the antisymmetrized diagrammatic technique [26]. Extension of these rules to include generic $n$-particle interaction vertices is straightforward. Due to the use of an antisymmetrized interaction, the diagrams acquire a combinatorial prefactor. For a tuple of $n$ equivalent lines, the expression has to be multiplied by a factor $1/n!$. As simplest example we can write schematically the first self-energy correction of the diagram in Fig. 5, which contains a single closed loop

$$\tilde{\Sigma}^{(1)}_{12} = -T \sum_{34} \gamma_{1324}\, \tilde{G}^{\mathrm{loc}}_{43} \tag{34}$$

where $\tilde{G}^{\mathrm{loc}} = (1/N_k) \sum_{\mathbf{k}} \tilde{G}(\mathbf{k})$ denotes the local part of the dual Green function. The second-order contribution represented in Fig. 5 contains two equivalent lines and one closed loop, and

hence is k-dependent

$$\tilde{\Sigma}_{12}^{(2)}(\mathbf{k}) = -\frac{1}{2}\left(\frac{T}{N_k}\right)^2 \sum_{\mathbf{k}_1\mathbf{k}_2}\sum_{345678} \gamma_{1345}\, \tilde{G}_{57}(\mathbf{k}_1)\, \tilde{G}_{83}(\mathbf{k}_2)\, \tilde{G}_{46}(\mathbf{k}+\mathbf{k}_2-\mathbf{k}_1)\, \gamma_{6728}\ . \qquad (35)$$

In practice, it is more efficient to evaluate the lowest-order diagrams in real space and transform back to reciprocal space using the fast Fourier transform. After calculating the best possible series for the self-energy $\tilde{\Sigma}$ in the dual space one can calculate the renormalized Green function matrix for the original fermions using the following simple transformations [19]

$$G_\omega(\mathbf{k}) = \left[\left(g_\omega + g_\omega \tilde{\Sigma}_\omega(\mathbf{k}) g_\omega\right)^{-1} + \Delta_\omega - t_k\right]^{-1} \qquad (36)$$

which is a useful generalization of the DMFT Green's function (see Eq. (32)) to include non-local correlation effects.

The progress of the DMFT approach strongly depends on the development of efficient numerical solvers for an effective quantum impurity model.

# 4 Solving multiorbital quantum impurity problems

Even though DMFT reduces the extended lattice problem to a single-site problem, the solution of the underlying Anderson impurity model remains a formidable quantum many-body problem, which requires accurate solvers. Recently a new class of solvers has emerged, the continuous-time quantum impurity solvers. These are based on stochastic Monte-Carlo methods and mainly come in two different flavors: The weak and strong-coupling approach.

The weak-coupling or interaction expansion continuous-time (CT-INT) quantum Monte Carlo algorithm for fermions was originally introduced by Aleksei Rubtsov [27]. There are two main previous attempts: the first work by Nikolay Prokof'ev *et. al* [29], who devised a continuous-time scheme to sample the infinite series of Feynman diagrams for bosons, and a second work by Natalie Jachowicz and co-workers [30], who developed a continous-time lattice Monte Carlo algorithm using the Hubbard-Stratonovich decomposition. The power of new CT-QMC scheme is that it represents just the integration of the complex path integral without any transformation to effective non-interacting models and can be used for any compacted electron-electron vertex. We introduce the algorithm in the path integral formulation for the single-orbital Anderson impurity problem with a Hubbard-type interaction $Un_\uparrow n_\downarrow$. The generalization to the multiorbital case can be found in Ref. [20]. First, the action of the Anderson impurity model is divided into a Gaussian part $S_0$ and an interaction part $S_U$ as follows:

$$S_0 = \sum_\sigma \int_0^\beta d\tau \int_0^\beta d\tau' c_\sigma^*(\tau)\, \left[\partial_\tau - \mu + \Delta(\tau-\tau') + U\alpha_{-\sigma}(\tau)\delta(\tau-\tau')\right]\, c_\sigma(\tau')\ , \qquad (37)$$

$$S_U = U\int_0^\beta d\tau \left[c_\uparrow^*(\tau)c_\uparrow(\tau) - \alpha_\uparrow(\tau)\right]\left[c_\downarrow^*(\tau)c_\downarrow(\tau) - \alpha_\downarrow(\tau)\right]\ . \qquad (38)$$

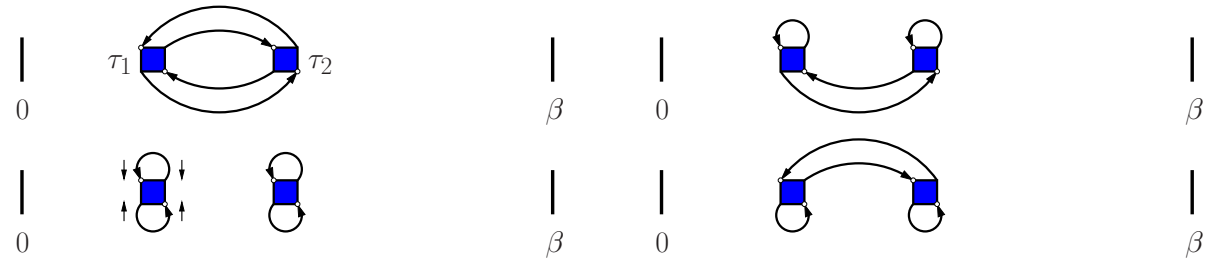


**Fig. 7:** *The four contributions to the partition function for $k = 2$. The interaction vertices are depicted by squares, bare Green functions as lines.*

The parameters $\alpha$ are introduced to control the sign problem. A formal series expansion for the partition function is obtained by expanding the exponential in the interaction term,

$$\mathcal{Z} = \int \mathcal{D}[c^*, c]\, e^{-S_0[c^*,c]} \sum_{k=0}^{\infty} \frac{(-1)^k}{k!} U^k \int_0^\beta d\tau_1 \ldots \int_0^\beta d\tau_k \, [c^*_\uparrow(\tau_1)c_\uparrow(\tau_1) - \alpha_\uparrow(\tau_1)] \tag{39}$$
$$\times [c^*_\downarrow(\tau_1)c_\downarrow(\tau_1) - -\alpha_\downarrow(\tau_1)] \ldots [c^*_\uparrow(\tau_k)c_\uparrow(\tau_k) - \alpha_\uparrow(\tau_k)][c^*_\downarrow(\tau_k)c_\downarrow(\tau_k) - \alpha_\downarrow(\tau_k)] \, .$$

Using the definition of the average over the noninteracting action

$$\langle ... \rangle_0 = \frac{1}{\mathcal{Z}_0} \int \mathcal{D}[c^*, c] ... \exp(-S_0), \tag{40}$$

the partition function can be expressed in the following form

$$\mathcal{Z} = \mathcal{Z}_0 \sum_{k=0}^{\infty} \int_0^\beta d\tau_1 \ldots \int_{\tau_{k-1}}^\beta d\tau_k \, \mathrm{sgn}(\Omega_k) \, |\Omega_k| \, , \tag{41}$$

where the integrand is given by

$$\Omega_k = (-1)^k U^k \langle [c^*_\uparrow(\tau_1)c_\uparrow(\tau_1) - \alpha_\uparrow(\tau_1)][c^*_\downarrow(\tau_1)c_\downarrow(\tau_1) - \alpha_\downarrow(\tau_1)] \ldots$$
$$\ldots [c^*_\uparrow(\tau_k)c_\uparrow(\tau_k) - \alpha_\uparrow(\tau_k)][c^*_\downarrow(\tau_k)c_\downarrow(\tau_k) - \alpha_\downarrow(\tau_k)] \rangle_0 \, . \tag{42}$$

Note that here the range of time integration has been changed such that time ordering is explicit: $\tau_1 < \ldots < \tau_{k-1} < \tau_k$. For a given set of times all $k!$ permutations of this sequence contribute to Eq. (39). These can be brought into the standard sequence by permuting quadruples of Grassmann numbers, and hence without gaining an additional sign. Since all terms are subject to time-ordering, their contribution to the integral is identical, so that the factor $1/k!$ in Eq. (39) cancels. A configuration can be fully characterized by specifying a perturbation-order $k$ and a set of $k$ times: $C_k = \{\tau_1, \ldots, \tau_k\}$.

The Monte Carlo algorithm performs importance sampling over this configuration space. The weight of a configuration is thereby taken to be equal to the modulus of the integrand, Eq. (42). Since $S_0$ is Gaussian, the average over the noninteracting system can be evaluated using Wick's theorem. Hence the weight of a configuration is essentially given by a fermionic determinant of a matrix containing the bare Green functions

$$\Omega_k = (-1)^k U^k \prod_\sigma \det \hat{g}^\sigma, \tag{43}$$

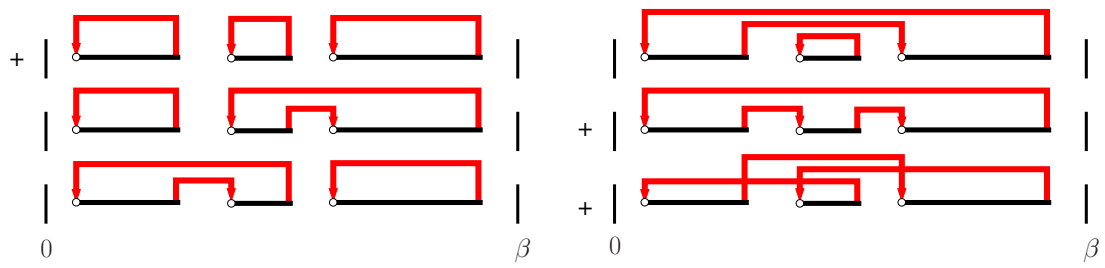


**Fig. 8:** *Diagrammatic representation of the six contributions to the partition function for spinless fermions at $k = 3$. An electron is inserted at the start of a segment (marked by an open circle) and removed at the segment endpoint. The hybridization function lines $\Delta(\tau_i - \tau'_j)$ (shown in red) are connected to the segments in all possible ways. The sign of each diagram is given on the left. (Reproduced from Ref. [28].)*

where the local Green function in the $\alpha$ fields is equal to

$$(\hat{g}^{\sigma})_{ij} = g_0^{\sigma}(\tau_i - \tau_j) - \alpha_{\sigma}(\tau_i)\delta_{ij} \; . \tag{44}$$

Note that determinants for different spin-orientations factorize, since the Green function is diagonal in spin-space.

The hybridization expansion (CT-HYB) or strong-coupling algorithm was initially introduced by Philipp Werner *et al.* [28] and has been generalized to multiorbital systems with general interactions [31, 32]. Here the algorithm is discussed in the segment representation, which exploits the possibility of a very fast computation of the trace for a density-density type of interaction. The action is regrouped into the atomic part

$$S_{\rm at} = \int_0^{\beta} d\tau \sum_{\sigma} c^*_{\sigma}(\tau) \left[\partial_{\tau} - \mu\right] c_{\sigma}(\tau) + U \int_0^{\beta} d\tau \, c^*_{\uparrow}(\tau) c_{\uparrow}(\tau) c^*_{\downarrow}(\tau) c_{\downarrow}(\tau) \tag{45}$$

and the part of the action $S_{\Delta}$ which contains the hybridization term

$$S_{\Delta} = -\int_0^{\beta} d\tau' \int_0^{\beta} d\tau \sum_{\sigma} c_{\sigma}(\tau) \Delta(\tau - \tau') \, c^*_{\sigma}(\tau') \, . \tag{46}$$

Here the sign is taken out by reversing the original order of $c$ and $c^*$ to avoid an alternating sign in the expansion. To simplify the notation, consider first the spinless-fermion model, which is obtained by disregarding the spin sums and interaction in Eqs. (45) and (46). The series expansion for the partition function is generated by expanding in the hybridization term:

$$\begin{aligned} \mathcal{Z} = \int \mathcal{D}[c^*, c] \, e^{-S_{\rm at}} \sum_k \frac{1}{k!} \int_0^{\beta} d\tau'_1 \int_0^{\beta} d\tau_1 \ldots \int_0^{\beta} d\tau'_k \int_0^{\beta} d\tau_k \times \\ \times \, c(\tau_k) c^*(\tau'_k) \ldots c(\tau_1) c^*(\tau'_1) \Delta(\tau_1 - \tau'_1) \ldots \Delta(\tau_k - \tau'_k). \end{aligned} \tag{47}$$

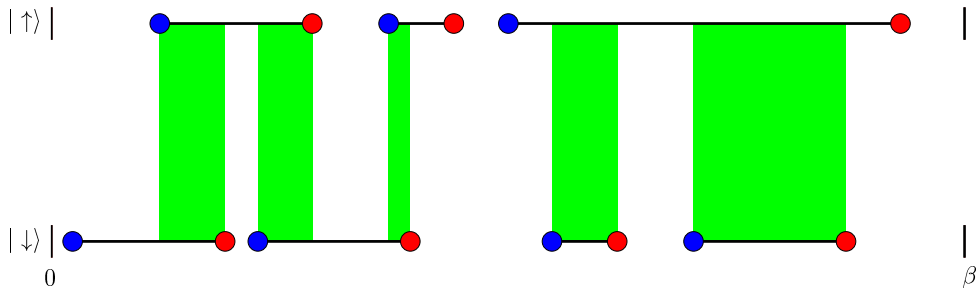


**Fig. 9:** *Example single-band CT-HYB in a segment picture: blue dots illustrate a creation operator, red ones annichilation operators and the black line represents the hybridization function $\Delta(\tau_i - \tau'_j)$. The green regions represent the time interval at which two electrons are present on the impurity with the total time $l_d$ and the price $U$ has to be paid.*

The important observation now is that, at any order, the diagrams can be collected into a determinant of hybridization functions. The partition function then takes the form

$$\mathcal{Z} = \mathcal{Z}_{\text{at}} \sum_k \int_0^\beta d\tau'_1 \int_{\tau'_1}^\beta d\tau_1 \ldots \int_{\tau_{k-1}}^\beta d\tau'_k \int_{\tau'_k}^{\circ\tau'_k} d\tau_k \, \langle c(\tau_k) c^*(\tau'_k) \ldots c(\tau_1) c^*(\tau'_1) \rangle_{\text{at}} \, \det \hat{\Delta}^{(k)}, \quad (48)$$

where the average is over the states of the atomic problem described by $S_{\text{at}}$. Here $\det \hat{\Delta}^{(k)}$ denotes the determinant of the matrix of hybridizations $\hat{\Delta}_{ij} = \Delta(\tau_i - \tau'_j)$. The diagrams contributing to the partition function for $k = 3$ are shown in Fig. 8. A diagram is depicted by a collection of segments, where a segment is symbolic for the time interval where the impurity is occupied. The collection of diagrams obtained by connecting the hybridization lines in all possible ways corresponds to the determinant. Collecting the diagrams into a determinant is essential to alleviate, or completely suppress the sign problem. Note that the imaginary-time interval in Eq. (48) is viewed as a circle denoted by $\circ\tau'_k$. The trajectories in the path integral are subject to antiperiodic boundary conditions which is accommodated by an additional sign if a segment winds around the circle.

For the single-orbital Anderson impurity model with Hubbard interaction the segment picture still holds and gives a very intuitive picture of the imaginary time dynamics. A configuration is visualized by two separate timelines, one for each spin. The additional sum over spins, $\sum_{\sigma_1 \ldots \sigma_k}$, which enters in the first line of Eq. (48), generates contributions such as the one shown in Fig. 9. The only difference to the spinless-fermion model is, that when the impurity is doubly occupied, the energy $U$ has to be paid and the trace is $e^{\mu(l_\uparrow + l_\downarrow) - U l_d}$, where $l_\sigma$ is the time spent on the impurity for an electron with spin $\sigma$ and $l_d$ is the time the impurity is doubly occupied.

In the Fig. 10 shows the comparison of CT-INT and CT-HYB for the strong-coupling case $U \geq W$ of single-band model. The perfect agreement of these two complementary CT-QMC schemes gives evidence for the possibility of a numerically exact solution of the quantum impurity problem.

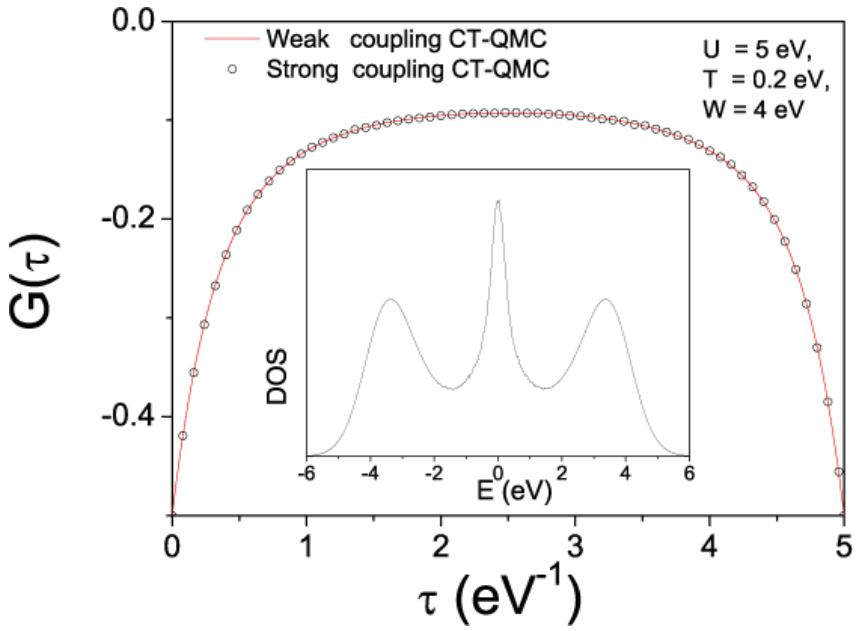


**Fig. 10:** *Comparison of the weak- (CT-INT) and strong-coupling (CT-HYB) CT-QMC impurity solvers for a one-band, semicircular model with $U \geq W$. The insert shows the density of states obtained with maximum entropy scheme.*

# 5 From models to real materials

In order to investigate real correlated systems with the local DMFT scheme, we need to have an efficient way of partitioning the spacial and orbital degrees of freedom. For example in the high-temperature superconducting oxide $YBa_2Cu_3O_7$, the strongly correlated electrons are Cu-$3d$, and, moreover, there is only one per non-equivalent copper $d_{x^2-y^2}$ band which crosses the Fermi level with strong many-body fluctuations. Just a few percent of the total number of electronic states need to be included in the DMFT calculations. Therefore the simplest realistic correlated scheme would be a DFT+DMFT approach [33, 34] with partitioning of the orbital space into normal band electrons $|K\rangle$ described by the DFT Bloch basis and correlated local orbitals $|L\rangle$ described by some optimal Wannier basis (see Fig. 11 for illustration).

The treatment of correlated electron systems requires the calculation of Green functions and hybridization functions in terms of local orbitals. This is readily achieved when using a basis set, which is localized in real space, such as linear (or $N$-th order) muffin-tin orbitals (NMTO) [35] or Gaussian basis sets [37]. However, many implementations of the density functional theory use a delocalized plane-wave basis set. This has the advantage, that the basis set is simple, universal, and its convergence is controlled in principle by a single parameter, the energy cutoff. The projector augmented wave method (PAW) [38], being a representative of a plane-wave based methods, can be used as a simple example of the general projection scheme from the Bloch to the local basis: $\langle K|L\rangle$.

Following the general projection scheme of Ref. [36,37], the desired quantity for an implementation of a DFT+DMFT method is a projection $\mathcal{P}^{\mathcal{C}} = \sum_L |L\rangle\langle L|$ of the full DFT Kohn-Sham

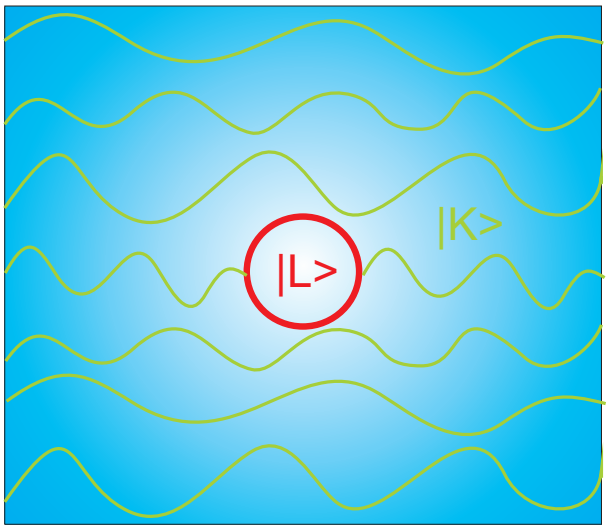


**Fig. 11:** *Schematic representation of the projection from a Bloch basis to a local Wannier correlated subset.*

Green function $G_{\mathrm{KS}}(\omega)$ on a set of localized orbitals $\{|L\rangle\}$

$$G^{\mathcal{C}}(\omega) = \mathcal{P}^{\mathcal{C}} G^{\mathrm{KS}}(\omega) \mathcal{P}^{\mathcal{C}}. \tag{49}$$

The subspace $\mathcal{C} = \mathrm{span}(\{|L\rangle\})$ is usually called correlated subspace. It is the subspace of orbitals in which many-body fluctuations play a major role and where the DMFT corrections to the DFT will be considered. In plane-wave based calculations, $G^{\mathrm{KS}}(\omega)$ in Matsubara space is available in terms of an almost complete set of Bloch states $|K\rangle$ that are eigenstates of the Kohn-Sham Hamiltonian $H_{\mathrm{KS}}|K\rangle = \varepsilon_K|K\rangle$:

$$G_{\mathrm{KS}}(\omega) = \sum_K \frac{|K\rangle\langle K|}{i\omega + \mu - \varepsilon_K}\,. \tag{50}$$

Inserting equation (50) into equation (49) shows that one needs to evaluate projections of the type $\langle L|K\rangle$ in order to access the matrix elements $G^{\mathcal{C}}_{LL'}(\omega)$ of the local Green function. In most cases the correlated orbitals are $d$- or $f$-orbitals, which are localized inside the PAW augmentation spheres to a good approximation. For $|L\rangle$ within these spheres and given the PAW decomposition [38] of a Bloch state $|K\rangle$ one obtains

$$\langle L|K\rangle = \sum_i \langle L|\phi_i\rangle\langle\tilde{p}_i|\tilde{K}\rangle.$$

The index $i$ of the augmentation functions $|\phi_i\rangle$ includes site $s$, angular momentum $l$, and $m$ as well as an index $\nu$ labeling the radial function: $i = (s, l, m, \nu)$. $|\tilde{p}_i\rangle$ are the PAW projectors.
In the described projection scheme the $|L\rangle\langle L|$ matrices are not properly normalized for two reasons: (1) the Bloch basis is incomplete since only a limited number of Bloch bands is included and (2) the PAW augmentation functions are, in general, not orthonormal. The simplest way is to orthonormalize the projection matrices by the following Wannier-type construction: By definition, the localized states $|L\rangle$ are labeled by site and angular-momentum indices: $L = (s, l, m)$.

We split the site index $s = \mathbf{R} + \mathbf{T}$ such that $\mathbf{R}$ labels the position within the unit cell and $\mathbf{T}$ is the Bravais lattice vector of the unit cell in which $s$ is located. This allows us to construct the Bloch transform of the localized states

$$|L_{\mathbf{k}}\rangle = \sum_{T} e^{i\mathbf{k}\mathbf{T}} |L_{\mathbf{T}}\rangle, \tag{51}$$

where $\mathbf{k}$ is from the first Brillouin zone and $|L_{\mathbf{T}}\rangle \equiv |L\rangle = |s, l, m\rangle$. The sum in equation (51) runs over the Bravais lattice. Labeling the Bloch states $|K\rangle = |\mathbf{k}, n\rangle$ by their crystal momentum, $\mathbf{k}$, and band index, $n$, we normalize our projection matrices $\mathcal{P}^{\mathcal{C}}_{Ln}(\mathbf{k}) = \langle L_{\mathbf{k}}|\mathbf{k}, n\rangle$ using the overlap operator

$$O_{LL'}(\mathbf{k}) = \sum_{n} \mathcal{P}^{\mathcal{C}}_{Ln}(\mathbf{k}) \mathcal{P}^{*\mathcal{C}}_{L'n}(\mathbf{k}) \tag{52}$$

in

$$\bar{\mathcal{P}}^{\mathcal{C}}_{Ln}(\mathbf{k}) = \sum_{L'} O^{-1/2}_{LL'}(\mathbf{k}) P^{\mathcal{C}}_{L'n}(\mathbf{k}). \tag{53}$$

These orthonormalized projection matrices are calculated once at the beginning of any calculation and can then be used to obtain the local Green function of the correlated orbitals from the full Bloch Green function $G^{B}_{nn'}$

$$G^{\mathcal{C}}_{LL'}(\omega) = \sum_{\mathbf{k},nn'} \bar{\mathcal{P}}^{\mathcal{C}}_{Ln}(\mathbf{k}) G^{B}_{nn'}(\mathbf{k}, \omega) \bar{\mathcal{P}}^{*\mathcal{C}}_{L'n'}(\mathbf{k}).$$

Similarly the hybridization function, $\Delta(\omega)$, is available. It is related to the local Green function by

$$G^{-1}(\omega) = i\omega - \epsilon_d - \Delta(\omega), \tag{54}$$

where $\epsilon_d$ is the static crystal field. Equation (54) is a matrix equation with $G$, $\Delta$, and $\epsilon_d$ being $\dim \mathcal{C} \times \dim \mathcal{C}$ matrices, in general. To separate the hybridization from the static DFT crystal field, we numerically evaluate the limit $\omega \to \infty$, where $\omega - G^{-1}(\omega) \to \epsilon_d$.
In a DFT+DMFT calculation the projection matrices $\bar{\mathcal{P}}^{\mathcal{C}}_{Ln}(k)$ are used for up- and down-folding quantities like the Green function and the self-energy in the course of the iterative DMFT procedure in exactly the same way as shown for the local Green function above. For example, the self-energy obtained by an impurity solver for the effective impurity model $\Sigma^{\mathcal{C}}_{LL'}(\omega)$ can be upfolded to the Bloch basis as follows

$$\Sigma^{B}_{nn'}(\mathbf{k}, \omega) = \sum_{LL'} \overline{P}^{*\mathcal{C}}_{Ln}(\mathbf{k}) \; \Sigma^{\mathcal{C}}_{LL'}(\omega) \; \overline{P}^{\mathcal{C}}_{L'n'}(\mathbf{k}) \, .$$

Since the self-energy in DMFT is a purely local quantity, the index $\mathbf{k}$ on $\Sigma^{B}_{nn'}(\mathbf{k}, \omega)$ reflects the momentum dependence brought about by the projection matrices. The presented projection scheme allows for the inclusion of both correlated and uncorrelated states in the procedure. Therefore, information about the interplay of correlated orbitals with their uncorrelated ligands can be obtained. As example, we show a realistic DFT+DMFT calculation of the $SrVO_3$ spectral function in the Fig. 12, were one can see the renormalisation of the valence correlated V-$t_{2g}$ states as well as broadening of the Bloch O-$2p$ states [39].

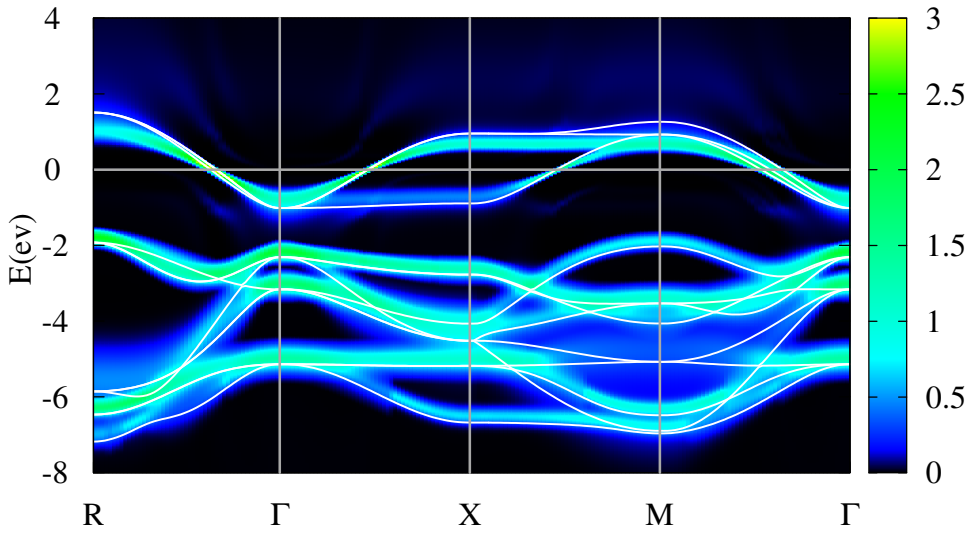


**Fig. 12:** *Momentum resolved impurity spectral function of $SrVO_3$ obtained by DFT+DMFT. The LDA band-structure of the V-$t_{2g}$ and O-$2p$ Bloch states is shown for comparison.*

# 6 Summary and outlook

We have learnt from simple model investigations how to treat electronic correlations within the local DMFT scheme. This knowledge can be used in realistic DFT+DMFT calculations for strongly correlated transition metals and rare earth systems, where the spin, orbital and charge fluctuations in the $d$- of $f$-shell play the crucial role for the photoemission spectrum as well as magnetic and optical excitations. The numerically exact solution of the quantum impurity problem gives us an effective local exchange-correlation functional for a given correlation material in a specific external field. Moreover, we have shown a direct way to include effects of non-local fluctuations in terms of a renormalized, locally screened dual perturbation scheme. The combination with first-principle approaches still offers many challenging problems.

# Acknowledgment

Support of the Deutsche Forschungsgemeinschaft through FOR1346 is gratefully acknowledged.

# References


[1] P. Hohenberg and W. Kohn, Phys. Rev. **136**, B864 (1964)

[2] W. Kohn and L.J. Sham, Phys. Rev. **140**, A1133 (1965)

[3] D.M. Ceperley and B.J. Alder, Phys. Rev. Lett. **45**, 566 (1980)

[4] G. Ortiz and P. Ballone, Phys. Rev. B **50**, 1391 (1994)

[5] E.K.U. Gross and W. Kohn, Adv. Quantum Chem. **21**, 255 (1990)

[6] R. O. Jones and O. Gunnarsson, Rev. Mod. Phys. **61**, 689 (1989)

[7] V.I. Anisimov, F. Aryasetiawan, and A.I. Lichtenstein, J. Phys.: Condens. Matter **9**, 767 (1997)

[8] A. Damascelli, Z. Hussain, and Z.-X. Shen, Rev. Mod. Phys. **75**, 473 (2003), G. Kotliar and D. Vollhardt, Physics Today **57**, 53 (2004)

[9] L. de Medici, J. Mravlje, and A. Georges, Phys. Rev. Lett. **107**, 256401 (2011)

[10] G. Kotliar, S.Y. Savrasov, K. Haule, V.S. Oudovenko, O. Parcollet, and C.A. Marianetti, Rev. Mod. Phys. **78**, 865 (2006)

[11] A.B. Migdal: *Theory of finite Fermi Systems and applications to atomic nuclei* (Interscience Publishers, New York, 1967)

[12] P. Nozières: *Theory of interacting Fermi systems* (Benjamin, New York, 1964)

[13] G. Baym and L.P. Kadanoff, Phys. Rev. **124**, 287 (1961)

[14] M. Potthoff, Eur. Phys. J. B **32**, 429 (2003)

[15] R. van Leeuwen, N.E. Dahlen, and A. Stan Phys. Rev. B **74**, 195105 (2006)

[16] A.N. Rubtsov, M.I. Katsnelson, and A.I. Lichtenstein, Phys. Rev. B **77**, 033101 (2008)

[17] H. Hafermann, F. Lechermann, A.N. Rubtsov, M.I. Katsnelson, A. Georges, and A.I. Lichtenstein, Lecture Notes in Physics **843**, 145 (2012), D.C. Cabra, A. Honecker, and P. Pujol (eds.): *Modern Theories of Many-Particle Systems in Condensed Matter Physics* (Springer, Berlin 2012)

[18] H. Hafermann, S. Brener, A.N. Rubtsov, M.I. Katsnelson, A.I. Lichtenstein, JETP Lett. **86**, 677 (2007)

[19] A.N. Rubtsov, M.I. Katsnelson, and A.I. Lichtenstein, Annals Phys. **327**, 1320 (2012)

[20] E. Gull, A.J. Millis, A.I. Lichtenstein, A.N. Rubtsov, M. Troyer, and P. Werner, Rev. Mod. Phys. **83**, 349 (2011)

[21] H. Hafermann, G. Li, A.N. Rubtsov, M.I. Katsnelson, A.I. Lichtenstein, and H. Monien, Phys. Rev. Lett. **102**, 206401 (2009)

[22] A. Georges, G. Kotliar, W. Krauth, and M.J. Rozenberg, Rev. Mod. Phys. **68** , 13 (1996)

[23] W. Metzner and D. Vollhardt, Phys. Rev. Lett. **62**, 324 (1989)

[24] E. Pavarini, E. Koch, and A.I. Lichtenstein, Phys. Rev. Lett. **101**, 266405 (2008)

[25] A.N. Rubtsov, M.I. Katsnelson, A.I. Lichtenstein, and A. Georges, Phys. Rev. B **79**, 045133 (2009)

[26] A.A. Abrikosov, L.P. Gorkov, and I.E. Dzyaloshinskii: *Methods of Quantum Field Theory in Statistical Physics* (Pergamon Press, New York, 1965)

[27] A.N. Rubtsov and A.I. Lichtenstein, JETP Lett. **80**, 61 (2004)

[28] P. Werner, A. Comanac, L. deMedici, M. Troyer, and A.J. Millis, Phys. Rev. Lett. **97**, 076405 (2006)

[29] N.V. Prokofev, B.V. Svistunov, and I.S. Tupitsyn, JETP Sov. Phys. **87**, 310 (1998)

[30] S.M.A. Rombouts, K. Heyde, and N. Jachowicz Phys. Rev. Lett. **82**, 4155 (1999)

[31] P. Werner and A.J. Millis, Phys. Rev. B **74**, 155107 (2006)

[32] K. Haule, Phys. Rev. B **75**, 155113 (2007)

[33] V.I. Anisimov, A.I. Poteryaev, M.A. Korotin, A.O. Anokhin, and G. Kotliar, J. Phys.: Condensed Matter **9**, 7359 (1997)

[34] A.I. Lichtenstein and M.I. Katsnelson, Phys. Rev. B **57**, 6884 (1998)

[35] O.K. Andersen and T. Saha-Dasgupta, Phys. Rev. B **62**, R16219 (2000)

[36] V.I. Anisimov, D.E. Kondakov, A.V. Kozhevnikov, I.A. Nekrasov, Z.V. Pchelkina, J.W. Allen, S.-K. Mo, H.-D. Kim, P. Metcalf, S. Suga, A. Sekiyama, G. Keller, I. Leonov, X. Ren and D. Vollhardt, Phys. Rev. B **71**, 125119 (2005)

[37] F. Lechermann, A. Georges, A. Poteryaev, S. Biermann, M. Posternak, A. Yamasaki and O.K. Andersen, Phys. Rev. B **74**, 125120 (2005)

[38] P. E. Blöchl, Phys. Rev. B **50**, 17953 (1994)

[39] M. Karolak, T.O. Wehling, F. Lechermann and A.I. Lichtenstein, J. Phys.: Condens. Matter **23**, 085601 (2011)